European Journal of Mechanics / A Solids 111 (2025) 105501

Contents lists available at ScienceDirect

European Journal of Mechanics / A Solids

journal homepage: www.elsevier.com/locate/ejmsol

Full length article

Simulation of anisotropic behaviour in additively manufactured structures using a curvilinear coordinate based finite element formulation

Bruno Musil *, Philipp Höfer

University of the Bundeswehr in Munich, Institute of Lightweight Engineering, Werner-Heisenberg-Weg 39, Neubiberg, 85579, Bavaria, Germany

ARTICLE INFO

Keywords:
Curvilinear coordinates
Anisotropy
Additive manufacturing
FEM

ABSTRACT

The advent of additive manufacturing has profoundly transformed component production. However, anisotropic structural behaviour is frequently observed in additively manufactured components, despite the isotropic nature of the constituent materials. This behaviour can be attributed to the manufacturing process, which involves the extrusion and deposition of individual material paths or the powder-based melting of such paths. For example, fused deposition modelling is a common technique employed in the production of polymer components. Technological advancements have enabled the use of fibre reinforcement, which can further amplify anisotropic material behaviour.

Several computational models and approaches have been proposed for simulating and optimising additively manufactured components treated as an anisotropic continuum. Current methods rely on a finite element discretisation of the continuum, where the print paths are assumed to be linear within a finite element. However, since the print paths are essentially arbitrary curves, a fine discretisation is necessary to achieve realistic simulations.

In this work, we propose a curvilinear local approach, where the print paths at the element level are considered to be curvilinear. The fineness of the mesh used in this concept depends solely on the stress gradients that need to be resolved. Furthermore, curvilinear print paths represent the coordinate lines used to describe anisotropy. As a result, the solution to the balance of linear momentum occurs within the local curvilinear coordinate system. This paper presents the implementation of this approach within the finite element method, using an exemplary boundary value problem.

1. Introduction

The field of additive manufacturing is experiencing a notable surge in prominence as a production technology across a diverse array of industrial sectors, particularly due to its capacity to generate intricate structural designs. Among the various additive manufacturing technologies, the material extrusion process has become the most established. The application is straightforward, the technology is relatively uncomplicated, the process is economically viable, and a diverse range of materials is available. The high degree of design freedom afforded by extrusion processes, when considered alongside their economic accessibility and the availability of high-performance materials, makes them the optimal choice for producing lightweight structures created through topology optimisation (cf. Lachmeyer et al., 2016). Fused deposition modelling represents a specific form of the extrusion process, whereby thermoplastic filament is applied in a layer-by-layer manner (cf. VDI 3405, 2014). Unlike other additive manufacturing processes, such as laser sintering or stereolithography, fused deposition modelling (FDM) enables the alignment of materials at the local level with a high degree of precision (cf. Parandoush and Lin, 2017). This local alignment results in material anisotropy (cf. Kafle et al., 2021, Kiendl and Gao, 2020). The use of fibre-reinforced filaments can further amplify the anisotropic effects (cf. Klingenbeck et al., 2024, Witzgall et al., 2022). In the FDM process, over 90% of the fibres are aligned in the direction of extrusion (cf. Tekinalp et al., 2014). A variety of optimisation techniques have been developed for the load-optimised design of print paths (cf. Fang et al., 2024, Fernandez et al., 2019, 2021, Murugan et al., 2022b,a), which is particularly important for the additive manufacturing of topology-optimised lightweight structures (cf. Voelkl and Wartzack, 2021). The print paths are represented by arbitrary curves and are thus not straight in general but exhibit curvature within the printed layer. It is crucial to note that the anisotropic structural-mechanical behaviour of additively manufactured components depends on several factors, particularly the selection of an appropriate domain in which the anisotropy can be characterised. The curvature of the print

* Corresponding author.
E-mail address: bruno.musil@unibw.de (B. Musil).

https://doi.org/10.1016/j.euromechsol.2024.105501
Received 16 August 2024; Accepted 13 November 2024
Available online 2 December 2024

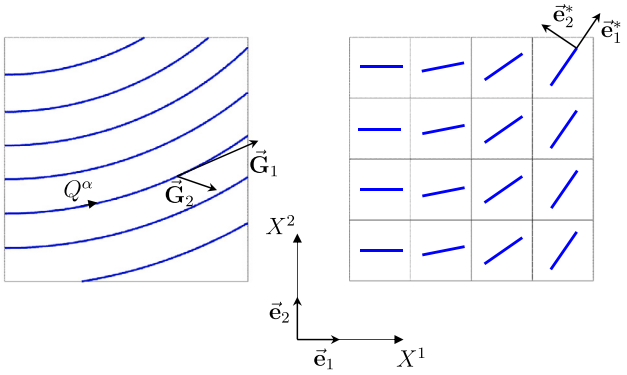

Fig. 1. Additively manufactured planar domain. Left: local approach; Right: global approach.

paths and the position of the domain within the component also have a substantial influence.

In the aforementioned publications, where anisotropic behaviour is simulated, the so-called "global approach" is employed, reflecting the current state of the art. Fig. 1 depicts a domain that has been additively manufactured using curved paths. In this illustration, the density of the print paths is decreased. To apply the global approach, it is first necessary to subdivide the domain into smaller elements, as illustrated in Fig. 1 on the right. In the context of an element, a straight print path with an orthonormal base system $\vec{\mathbf{e}}_i^*$ is assumed in principle. This allows for the consideration of orthotropic material behaviour within the aforementioned base system. The material properties are then transformed into the global Cartesian coordinate system X^i, where the governing equations are also solved. To simulate anisotropic material behaviour accurately, a very fine discretisation using finite elements is required, particularly for larger curvatures of the print paths.

To reduce the computational effort, it is possible to use only one element to discretise the domain rather than 16 elements as illustrated in Fig. 1. The print paths directly represent the coordinate lines Q^α of a curvilinear coordinate system in which the anisotropy is described. The space-dependent covariant basis vectors $\vec{\mathbf{G}}_\alpha$ are associated with this coordinate system. Furthermore, the governing equations are solved within the local curvilinear coordinate system. This idea, the so-called "local approach", is presented in detail within this paper, and a corresponding finite element formulation is developed.

In the context of the finite element method, Javili et al. (2014) and Valle et al. (2019) conducted an investigation into the utilisation of curvilinear coordinates and the formulation of curved finite elements. Cinefra (2022) developed a curved finite element, which represents a generalisation of the classical shell elements and allows for the possibility of curvature in the third direction. The strains were derived in the local curvilinear reference frame, analogous to the methodology employed in the present work. In the aforementioned studies, a methodology for the development of curved finite elements is presented, wherein the mesh geometry is assumed to be curved. The motivation for developing the element presented here is the application of the aforementioned "local approach" in the context of additively manufactured components. It is crucial that the meshing of the component geometry occurs independently of the underlying print paths, which is why the element does not necessitate curvilinear boundaries. Consequently, the meshing is conducted in the Cartesian coordinate system, while the physical description of the anisotropic continuum and the solution of the governing equations are performed in a curved configuration.

2. Fundamentals of the elasticity theory in curvilinear coordinates

This section briefly summarises the fundamentals of elasticity theory in curvilinear coordinates and derives certain continuum mechanical quantities that are relevant to this work. A detailed description and derivation of the theory can be found in the relevant literature (see Betten, 1987, Irgens, 2008; Irgens et al., 2019, Itskov et al., 2007, Klingbeil, 1966).

To describe the general motion of a deformable body in space, a set of Cartesian coordinates is defined for both the reference configuration, represented by the coordinates X^i, and the current configuration, represented by the coordinates x^i. The Cartesian coordinates of a material point in Euclidean space correspond to the components of the associated position vector of the same material point, represented as:

$$\begin{aligned} \vec{\mathbf{X}} &= \vec{\mathbf{X}}(X^i) \\ \vec{\mathbf{x}} &= \vec{\mathbf{x}}(x^i)\,. \end{aligned} \tag{1}$$

It should be noted that in the case of mathematical description using the curvilinear coordinates of the reference configuration Q^α or the current configuration q^α, the components of the position vector

$$\begin{aligned} \vec{\mathbf{X}} &= \vec{\mathbf{X}}(Q^\alpha) \\ \vec{\mathbf{x}} &= \vec{\mathbf{x}}(q^\alpha) \end{aligned} \tag{2}$$

do not correspond to the curvilinear coordinates of the material point and the following applies

$$\begin{aligned} \vec{\mathbf{X}} &= X_\alpha \vec{\mathbf{G}}^\alpha = X^\alpha \vec{\mathbf{G}}_\alpha = X_i \vec{\mathbf{e}}_i \\ \vec{\mathbf{x}} &= x_\alpha \vec{\mathbf{g}}^\alpha = x^\alpha \vec{\mathbf{g}}_\alpha = x_i \vec{\mathbf{e}}_i\,. \end{aligned} \tag{3}$$

Here, $\vec{\mathbf{G}}_\alpha$ and $\vec{\mathbf{G}}^\alpha$ are the co- and contravariant basis vectors of the reference configuration, $\vec{\mathbf{g}}_\alpha$ and $\vec{\mathbf{g}}^\alpha$ are the co- and contravariant basis vectors of the current configuration, and finally, $\vec{\mathbf{e}}_i$ is the orthonormal basis vector. As is customary in tensor algebra, all quantities related to curvilinear coordinates are indexed with Greek letters, and Cartesian quantities are indexed with Latin letters. Within the framework of the geometrically linear formulation, only the quantities of the reference configuration are considered in the following.

With regard to a transformation of the coordinates, the following is valid for the calculation of the base vectors

$$\begin{aligned} \vec{\mathbf{G}}_\alpha &= \frac{\partial X^i}{\partial Q^\alpha} \vec{\mathbf{e}}_i \\ \vec{\mathbf{G}}^\alpha &= \frac{\partial Q^\alpha}{\partial X^i} \vec{\mathbf{e}}_i \end{aligned} \tag{4}$$

and any tensor components

$$\begin{aligned} t_\alpha &= \frac{\partial X^i}{\partial Q^\alpha} t_i \\ t^\alpha &= \frac{\partial Q^\alpha}{\partial X^i} t_i\,. \end{aligned} \tag{5}$$

Using the appropriate form

$$\begin{aligned} G_{\alpha\beta} &= \vec{\mathbf{G}}_\alpha \cdot \vec{\mathbf{G}}_\beta \\ G^{\alpha\beta} &= \vec{\mathbf{G}}^\alpha \cdot \vec{\mathbf{G}}^\beta \\ G_\alpha^\beta &= \vec{\mathbf{G}}_\alpha \cdot \vec{\mathbf{G}}^\beta = \delta_\alpha^\beta \end{aligned} \tag{6}$$

of the metric tensor $\mathbf{G}$, rising or lowering of a component index is possible. The deformation gradient tensor in curvilinear coordinates is

$$\mathbf{F} = \frac{\partial \vec{\mathbf{X}}}{\partial Q^\alpha} + \frac{\partial \vec{\mathbf{u}}}{\partial Q^\alpha} \tag{7}$$

and in component notation

$$F_{\beta\alpha} = G_{\beta\alpha} + u_\beta|_\alpha\,. \tag{8}$$

The covariant derivative of the displacement field

$$u_\beta|_\alpha = \frac{\partial u_\beta}{\partial Q^\alpha} - \Gamma^\gamma_{\beta\alpha} u_\gamma \tag{9}$$

takes the space dependence of the basis vectors into account. Therefore, the Christoffel symbols of the second kind

$$\Gamma^\gamma_{\beta\alpha} = \frac{\partial \vec{\mathbf{G}}_\alpha}{\partial Q^\beta} \cdot \vec{\mathbf{G}}^\gamma \tag{10}$$

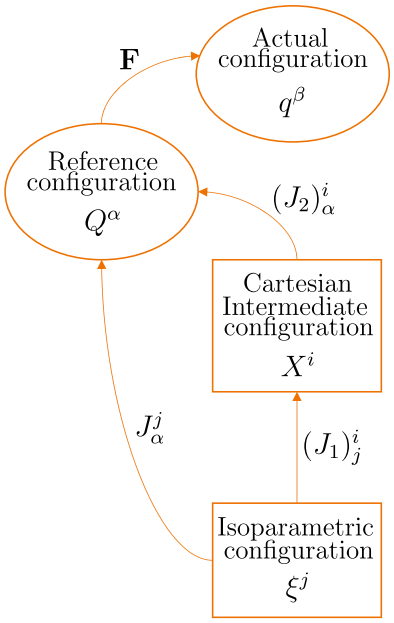

Fig. 2. Schematic representation of the mixed coordinate interpolation.

must be evaluated for the curvilinear coordinate system. In order to calculate the stress state, the deformation tensor

$$\mathbf{C} = \mathbf{F}^{\mathrm{T}} \cdot \mathbf{F} = F^\gamma_\alpha F_{\gamma\beta}\, \vec{\mathbf{G}}^\alpha \otimes \vec{\mathbf{G}}^\beta \tag{11}$$

of the reference configuration is first considered. Combining Eqs. (8) and (11), we obtain the following

$$\begin{aligned} \mathbf{E} &= \frac{1}{2}(\mathbf{C} - \mathbf{I}) \\ &= \frac{1}{2}\left(u_\alpha|_\beta + u_\beta|_\alpha + u^\gamma|_\alpha\, u_\gamma|_\beta\right) \vec{\mathbf{G}}^\alpha \otimes \vec{\mathbf{G}}^\beta \end{aligned} \tag{12}$$

for the Green–Lagrange strain tensor. Assuming linear elastic material behaviour

$$\sigma^{\alpha\beta} = \mathbb{C}^{\alpha\beta\mu\nu} E_{\mu\nu} \tag{13}$$

the fourth-order material tensor generally consists of 21 independent components and must be defined in material coordinates (i.e. in the curvilinear coordinate system). In the case of isotropy, the following applies

$$\mathbb{C}^{\alpha\beta\gamma\delta} = \lambda\, G^{\alpha\beta}\, G^{\gamma\delta} + \mu\left(G^{\alpha\gamma}\, G^{\beta\delta} + G^{\alpha\delta}\, G^{\beta\gamma}\right), \tag{14}$$

where λ and μ are the Lamé constants. The quasi-static form of the balance of linear momentum

$$\int_\Omega \sigma^{\alpha\beta}\, \delta E_{\alpha\beta}\, dV = \int_{\partial\Omega} t^\alpha\, \delta u_\alpha\, dA, \tag{15}$$

represented in the weak formulation, is used to solve for the displacement field.

3. Finite element formulation

A concept of mixed coordinate interpolation is proposed in this paper (see Fig. 2). The motivation is that the spatial discretisation takes place in the Cartesian coordinate system

$$X^i = \sum_I {}^I N(\xi^j)\, {}^I X^i \tag{16}$$

and the fundamental finite element technology remains isoparametric. Thus, the finite element mesh is independent of the curved print paths. However, the solution of the physical problem and the description of the continuum take place in the curvilinear coordinate system. In Eq. (16) is N the shape function of the Ith node and ξ^j are the isoparametric coordinates. The displacement field

$$u_i = \sum_I {}^I N(\xi^j)\, {}^I u_i \tag{17}$$

is discretised in the same way. A key aspect is the formulation of the discrete covariant derivative, which is a prerequisite for the calculation of the strain field. By applying the transformation rule (Eq. (5))

$$u_\alpha = \frac{\partial X^i}{\partial Q^\alpha} u_i = (J_2)^i_\alpha\, u_i \tag{18}$$

to the displacement field and considering the aforementioned discretisation (Eq. (17)), Eq. (9) can be expressed as follows:

$$u_\beta|_\alpha = {}^I N\, {}^I u_i \frac{\partial}{\partial Q^\alpha}(J_2)^i_\beta + \frac{\partial\, {}^I N}{\partial Q^\alpha}\, {}^I u_i\, (J_2)^i_\beta - \Gamma^\gamma_{\beta\alpha}\, {}^I N\, {}^I u_j\, (J_2)^j_\gamma . \tag{19}$$

The derivatives of the shape functions with respect to the curvilinear coordinates

$$\frac{\partial\, {}^I N}{\partial Q^\alpha} = (J_1^{-1})^j_k\, (J_2)^k_\alpha \frac{\partial\, {}^I N}{\partial \xi^j} = J^j_\alpha \frac{\partial\, {}^I N}{\partial \xi^j} \tag{20}$$

can be calculated according to the chain rule. This includes

$$(J_1)^i_j = \frac{\partial X^i}{\partial \xi^j} = \frac{\partial\, {}^I N}{\partial \xi^j}\, {}^I X^i . \tag{21}$$

3.1. Numerical calculation of the Christoffel symbols

The Christoffel symbols are calculated numerically and independently of the selected curvilinear coordinate system. Consequently, various quantities must be calculated at the Gauss point level. The ith component of the covariant basis vector

$$\vec{\mathbf{G}}_\alpha = J^j_\alpha \frac{\partial\, {}^I N}{\partial \xi^j}\, {}^I X^i \tag{22}$$

can be calculated by combining Eq. (4), Eq. (16) and (20). Subsequently, the covariant metric tensor

$$G_{\alpha\beta} = \vec{\mathbf{G}}_\alpha \cdot \vec{\mathbf{G}}_\beta \tag{23}$$

and its inverse, the contravariant metric tensor $G^{\alpha\beta}$, can be calculated. The contravariant base system is thus obtained as follows

$$\vec{\mathbf{G}}^\alpha = G^{\alpha\beta}\, \vec{\mathbf{G}}_\beta . \tag{24}$$

In the following step, Eq. (22) can be inserted into the definition of the Christoffel symbols (Eq. (10)), and the differentiation with respect to the curvilinear coordinates Q^β is carried out. This leads to

$$\begin{aligned} \Gamma^\gamma_{\beta\alpha} = \Bigg[& J^j_\alpha J^k_\beta \frac{\partial^2\, {}^I N}{\partial \xi^j\, \partial \xi^k} + \\ & \left(\frac{\partial}{\partial Q^\beta}(J_1^{-1})^j_k\, (J_2)^k_\alpha + (J_1^{-1})^j_k \frac{\partial}{\partial Q^\beta}(J_2)^k_\alpha \right) \frac{\partial\, {}^I N}{\partial \xi^j} \Bigg]\, {}^I X^i\, (\vec{\mathbf{G}}^\gamma)_i . \end{aligned} \tag{25}$$

The following rule can be applied

$$\frac{\partial}{\partial Q^\beta}(J_1^{-1})^j_i = -(J_1^{-1})^k_i \frac{\partial}{\partial Q^\beta}(J_1)^m_k\, (J_1^{-1})^j_m \tag{26}$$

with

$$\frac{\partial}{\partial Q^\beta}(J_1)^k_j = \frac{\partial}{\partial Q^\beta}\left(\frac{\partial\, {}^I N}{\partial \xi^j}\, {}^I X^k\right) = J^m_\beta \frac{\partial^2\, {}^I N}{\partial \xi^j\, \partial \xi^m}\, {}^I X^k \tag{27}$$

to calculate the derivative of the inverse transformation with respect to the curvilinear coordinates. As can be observed in Eqs. (25) and (27), at least quadratic shape functions are required, as the second partial derivatives of the shape functions appear. In this paper, a quadratic Lagrangian element comprising nine nodes and nine Gauss points is employed to conduct the simulations presented in Chapter 4.

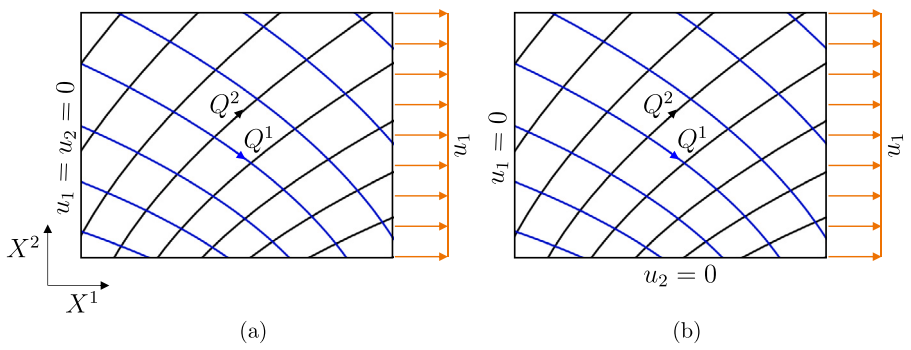

Fig. 3. (a) The first boundary value problem (BVP I) and (b) the second boundary value problem (BVP II) with prescribed boundary conditions.

3.2. Strain and stiffness matrix

Assuming small strains, the linearised strain tensor

$$\varepsilon_{\alpha\beta} = \frac{1}{2}\left(u_\alpha|_\beta + u_\beta|_\alpha\right) \tag{28}$$

of the element can be finally reformulated using the Voigt notation as

$$\boldsymbol{\varepsilon}^e = \mathbf{B}^e\,\mathbf{u}^e, \tag{29}$$

whereby

$$\mathbf{u}^e = \begin{pmatrix} {}^1u_1 & {}^1u_2 & \dots & {}^9u_1 & {}^9u_2 \end{pmatrix}^{\mathrm{T}} \tag{30}$$

is the vector of the nodal degrees of freedom of the element in Cartesian coordinates. The strain interpolation matrix of the element

$$\mathbf{B}^e = \mathbf{A}_1^e\,\mathbf{N}^e + \mathbf{A}_2^e\,\mathbf{B}_{\mathrm{N}}^e - \boldsymbol{\Gamma}^e\,\mathbf{A}_3^e\,\mathbf{N}^e \tag{31}$$

comprises three terms, analogous to the covariant derivative (Eq. (19)), with the matrices:

$$\mathbf{N}^e = \begin{pmatrix} {}^1N & 0 & {}^2N & 0 & \dots & {}^9N & 0 \\ 0 & {}^1N & 0 & {}^2N & \dots & 0 & {}^9N \end{pmatrix} \tag{32}$$

$$\mathbf{B}_{\mathrm{N}}^e = \begin{pmatrix} \frac{\partial\,{}^1N}{\partial Q^1} & 0 & \frac{\partial\,{}^2N}{\partial Q^1} & 0 & \dots & \frac{\partial\,{}^9N}{\partial Q^1} & 0 \\ 0 & \frac{\partial\,{}^1N}{\partial Q^1} & 0 & \frac{\partial\,{}^2N}{\partial Q^1} & \dots & 0 & \frac{\partial\,{}^9N}{\partial Q^1} \\ \frac{\partial\,{}^1N}{\partial Q^2} & 0 & \frac{\partial\,{}^2N}{\partial Q^2} & 0 & \dots & \frac{\partial\,{}^9N}{\partial Q^2} & 0 \\ 0 & \frac{\partial\,{}^1N}{\partial Q^2} & 0 & \frac{\partial\,{}^2N}{\partial Q^2} & \dots & 0 & \frac{\partial\,{}^9N}{\partial Q^2} \end{pmatrix} \tag{33}$$

$$\boldsymbol{\Gamma}^e = \begin{pmatrix} \Gamma^1_{11} & \Gamma^2_{11} \\ \Gamma^1_{22} & \Gamma^2_{22} \\ 2\,\Gamma^1_{12} & 2\,\Gamma^2_{12} \end{pmatrix} \tag{34}$$

$$\mathbf{A}_3^e = \begin{pmatrix} (J_2)^1_1 & (J_2)^2_1 \\ (J_2)^1_2 & (J_2)^2_2 \end{pmatrix} \tag{35}$$

$$\mathbf{A}_2^e = \begin{pmatrix} (J_2)^1_1 & (J_2)^2_1 & 0 & 0 \\ 0 & 0 & (J_2)^1_2 & (J_2)^2_2 \\ (J_2)^1_2 & (J_2)^2_2 & (J_2)^1_1 & (J_2)^2_1 \end{pmatrix} \tag{36}$$

$$\mathbf{A}_1^e = \begin{pmatrix} \frac{\partial}{\partial Q^1}(J_2)^1_1 & \frac{\partial}{\partial Q^1}(J_2)^2_1 \\ \frac{\partial}{\partial Q^2}(J_2)^1_2 & \frac{\partial}{\partial Q^2}(J_2)^2_2 \\ \frac{\partial}{\partial Q^2}(J_2)^1_1 & \frac{\partial}{\partial Q^2}(J_2)^2_1 \\ \frac{\partial}{\partial Q^1}(J_2)^1_2 & \frac{\partial}{\partial Q^1}(J_2)^2_2 \end{pmatrix} \tag{37}$$

By rewriting the weak formulation (Eq. (15)) in Voigt notation and inserting the discrete virtual strain $\delta\boldsymbol{\varepsilon}^e$ according to Eq. (29)

$$\mathbf{K}^e = \int_{\Omega_e} (\mathbf{B}^e)^{\mathrm{T}}\,\bar{\mathbf{C}}\,\mathbf{B}^e\,dV = \int_{\Omega_\square} (\mathbf{B}^e)^{\mathrm{T}}\,\bar{\mathbf{C}}\,\mathbf{B}^e\,\det(\mathbf{J}^e)\,dV_\square \tag{38}$$

one obtains the element stiffness matrix $\mathbf{K}^e$. In this equation, $\Omega_\square$ represents the isoparametric integration domain, such that the Gauss integration rule can be directly applied. Since the finite element mesh is not curvilinear but Cartesian, the element Jacobian $\mathbf{J}^e$ is equal to the transpose of $\mathbf{J}_1$, as defined in Eq. (21).

Table 1
Orthotropic material parameters.

E_1	$5 \cdot 10^4$	MPa
E_2	$2 \cdot 10^4$	MPa
E_3	$2 \cdot 10^4$	MPa
ν_{23}	0,4	
ν_{13}	0,3	
ν_{12}	0,3	
G_{23}	$2 \cdot 10^4$	MPa
G_{13}	$1 \cdot 10^4$	MPa
G_{12}	$1 \cdot 10^4$	MPa

4. Results and discussion

The finite element developed has been implemented in the commercial finite element software *ANSYS*, utilising the Fortran subroutine *UserElem*. This work involves the solution of a two-dimensional boundary value problem, as illustrated in Fig. 3. In the first boundary value problem (BVP I), the left edge is subjected to a clamped condition, whereas in the second boundary value problem (BVP II), homogeneous boundary conditions are imposed. In both cases, the displacement in the X_1-direction is prescribed at the right edge. In this example, an elliptical coordinate system

$$\begin{aligned} X^1 &= \cosh(Q^2)\,\cos(Q^1) \\ X^2 &= \sinh(Q^2)\,\sin(Q^1) \end{aligned} \tag{39}$$

is used to describe the print paths, which are coincident with the Q^1 coordinate lines. Hence, the transformation coefficients $(J_2)^i_\alpha$ are

$$\begin{aligned} (J_2)^1_1 &= -\cosh(Q^2)\,\sin(Q^1) \\ (J_2)^2_1 &= \sinh(Q^2)\,\cos(Q^1) \\ (J_2)^1_2 &= \sinh(Q^2)\,\cos(Q^1) \\ (J_2)^2_2 &= \cosh(Q^2)\,\sin(Q^1). \end{aligned} \tag{40}$$

For illustrative purposes, only a subset of the print paths is displayed in Fig. 3. The element stiffness matrix (Eq. (38)) contains the material tensor $\bar{\mathbf{C}}$ in Voigt notation. In order to verify the numerical implementation of the finite element, an isotropic material behaviour (Eq. (14)) was initially assumed. Consequently, the results, including the displacements, strains and stresses, prove to be independent of the curvature and shape of the print paths. To simulate anisotropy, orthotropic material behaviour is assumed. The material parameters are shown in Table 1.

4.1. Anisotropic simulation

The present study involved simulations of the aforementioned boundary value problems with varying finite element mesh refinement and different print path shapes. The objective was to compare the two calculation methods described in Chapter 1: the standard global approach and the newly developed local approach.

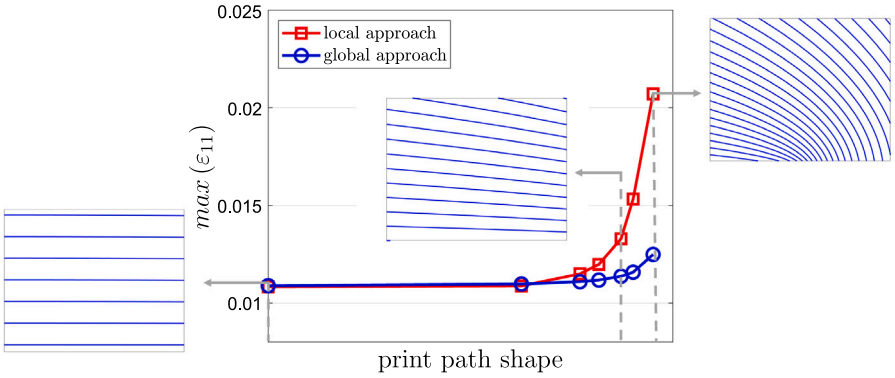

Fig. 4. Shape convergence study for BVP I.

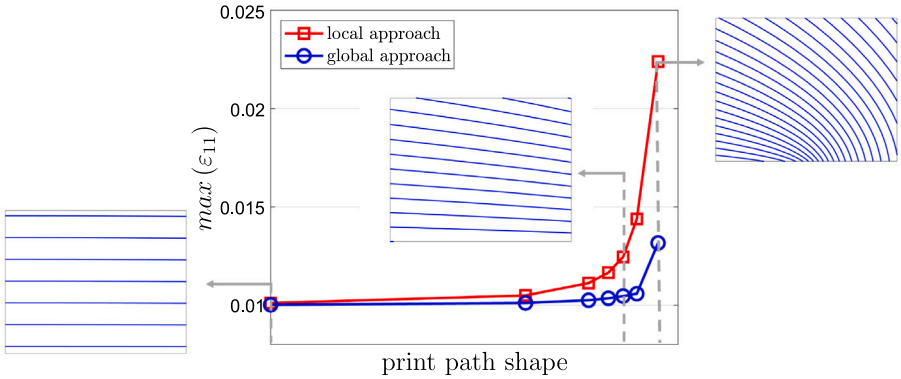

Fig. 5. Shape convergence study for BVP II.

The initial step was to vary the shape of the print paths within the domain of the component, while maintaining a constant finite element mesh. This is achieved by moving the domain along the elliptical coordinate system. For illustrative purposes, examples of the diverse shapes of the print paths are provided in Figs. 4 and 5. The maximum strain in the X_1-direction is then compared. The results indicate that the two approaches converge towards each other for small curvatures of the print paths. However, for larger curvatures, there is an evident discrepancy.

Subsequently, a comparative analysis was carried out concerning the strain fields associated with a constant form of the print paths. To gain further insight, a mesh convergence study was conducted. The outcomes for minor curvatures of the print paths, which are nearly linear, are presented in Fig. 6 for both boundary value problems. In this instance, the influence of the mesh refinement on the result is negligible, so that equivalence can be assumed. The corresponding strain fields can be observed in Figs. 7 and 8. Regarding BVP I, it can be observed that the strain fields have an identical shape. The maximum strains occur in the area of the clamped edges. In consideration of BVP II, it is evident that the strain fields display different forms in relation to each other. Nevertheless, the range of values for the minimum and maximum strain is relatively narrow, indicating that the two strain fields can be regarded as almost homogeneous. In the case of complete homogeneity of the strain field, it is necessary for the print paths to be aligned along the X_1 axis, without the presence of any minimum curvature. In contrast with the aforementioned results, a more complex form of print paths with pronounced curvatures is considered and analysed in the following. The results of the simulations are presented in Figs. 9–11. It can be observed that the strain fields exhibit different maximum values and behaviours. In the case of BVP I, the local approach demonstrates convergence to a constant value. In contrast, the global approach demonstrates a notable increase in maximum strains with mesh refinement. This phenomenon can be attributed to the fact that the maxima in the global approach are situated in the fixed corners, which represent a singularity point. In the local approach, the maximum strains occur at the point of maximum stiffness of the component. Qualitatively similar simulation results can be observed in the case of BVP II. As there is no longer a singularity, the global approach also converges to a constant value.

The numerical investigations raise the essential question of why there is a significant difference between the two calculation methods analysed, particularly for large curvatures of the print paths. The source of the issue can be traced back to the constitutive law. There is an incompatibility between the strain tensor and the material tensor. The strain tensor is accurate and provides the true values, taking into account the curvature due to the covariant derivative of the curvilinear displacement. However, the local approach necessitates that the material tensor can be determined experimentally in the local curvilinear coordinate system. Nevertheless, material characterisation is only feasible on unidirectional specimens in the Cartesian coordinate system. An additional transformation into the curvilinear coordinate system could be implemented to create the local material tensor; however, this would yield invariant results in terms of the shape and curvature of the print paths, which correspond to a solution for anisotropy in the global Cartesian coordinate system.

One straightforward solution to this problem is the introduction of

$$\vec{\mathbf{b}}_\alpha = \frac{\vec{\mathbf{G}}_\alpha}{\left|\vec{\mathbf{G}}_\alpha\right|} \tag{41}$$

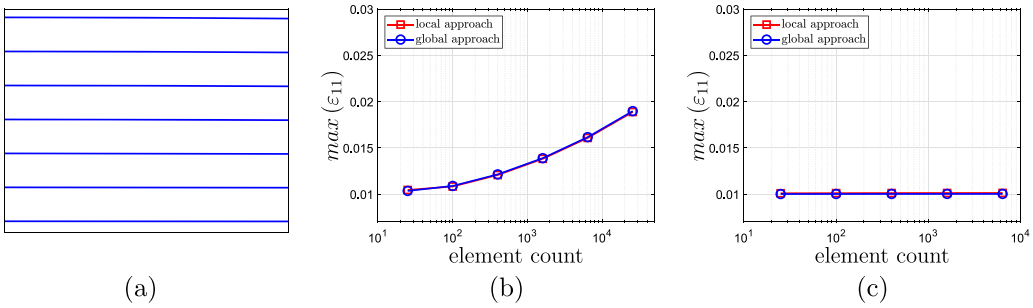

Fig. 6. Mesh convergence study for minimal curvatures of the print paths (a): (b) BVP I; (c) BVP II.

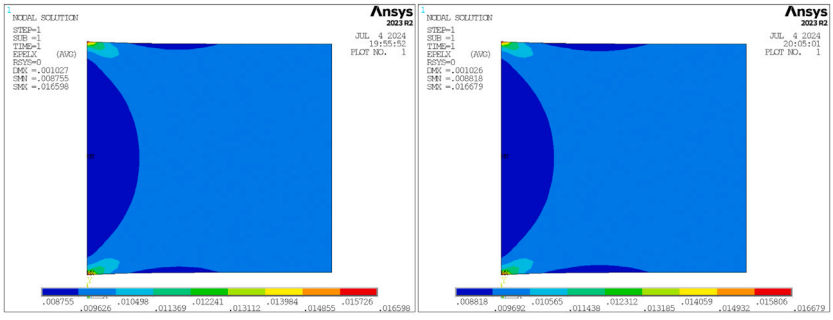

Fig. 7. Strain fields of the BVP I: (a) local approach; (b) global approach.

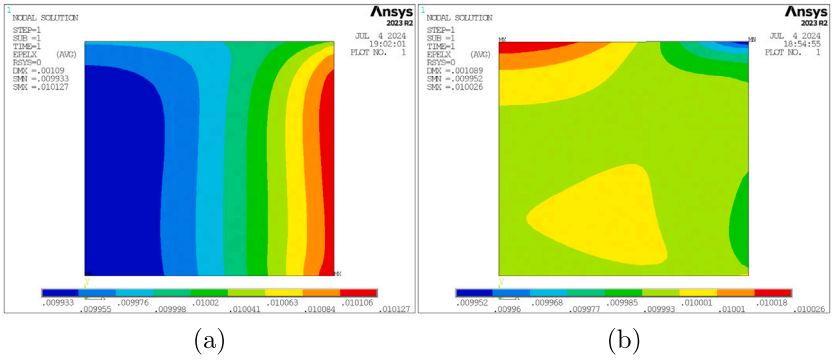

Fig. 8. Strain fields of the BVP II: (a) local approach; (b) global approach.

the normalised local basis system $\vec{\mathbf{b}}_\alpha$. Consequently, the transformation coefficients $(J_2)^i_\alpha$ are

$$
\begin{aligned}
(J_2)^1_1 &= \frac{-\cosh(Q^2)\sin(Q^1)}{\sqrt{\sinh^2(Q^2)\sin^2(Q^1)}} \\
(J_2)^2_1 &= \frac{\sinh(Q^2)\cos(Q^1)}{\sqrt{\sinh^2(Q^2)\sin^2(Q^1)}} \\
(J_2)^1_2 &= \frac{\sinh(Q^2)\cos(Q^1)}{\sqrt{\sinh^2(Q^2)\sin^2(Q^1)}} \\
(J_2)^2_2 &= \frac{\cosh(Q^2)\sin(Q^1)}{\sqrt{\sinh^2(Q^2)\sin^2(Q^1)}}\,.
\end{aligned}
\tag{42}
$$

With these adjustments, all the calculations presented in Section 3 can be performed. Thus, all the simulation results for both boundary value problems using the local approach with the normalised local basis agree exactly with the results of the global approach.

5. Conclusion

In the present work, a novel curvilinear coordinate-based finite element formulation is introduced for the simulation of anisotropic behaviour in additively manufactured structures. In contrast to conventional methodologies, which assume linear print paths within the finite elements, our approach considers the curvilinear nature of the print paths at the element level. A notable innovation is the mixed coordinate interpolation, whereby the spatial discretisation is conducted in the Cartesian coordinate system while the physical problem is solved in the local curvilinear coordinate system. The methodology presented herein enables the finite element mesh to be defined independently of the curved print paths, which are instead accurately represented by the local curvilinear coordinates.

The numerical calculation of the Christoffel symbols and the strain and stiffness matrices represents a significant challenge in this work. These are of crucial importance for the accurate modelling of the anisotropy. The finite element developed was implemented in the commercial finite element software *ANSYS* using the Fortran subroutine

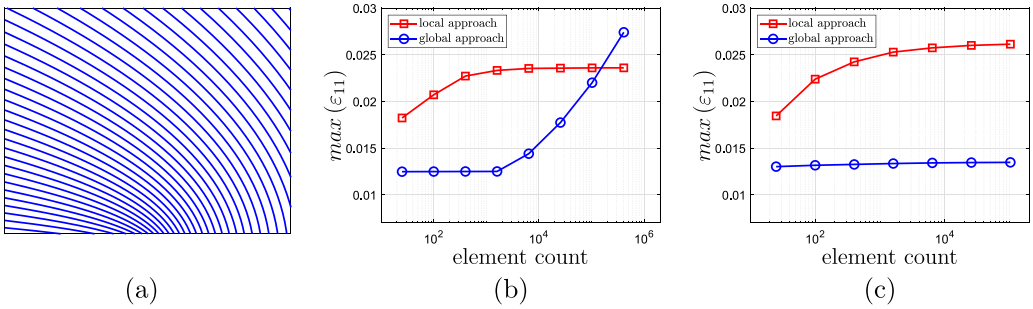

Fig. 9. Mesh convergence study for pronounced curvatures of the print paths (a): (b) BVP I; (c) BVP II.

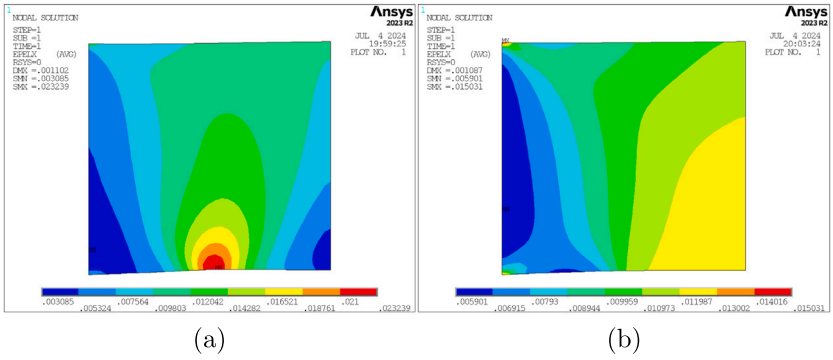

Fig. 10. Strain fields of the BVP I: (a) local approach; (b) global approach.

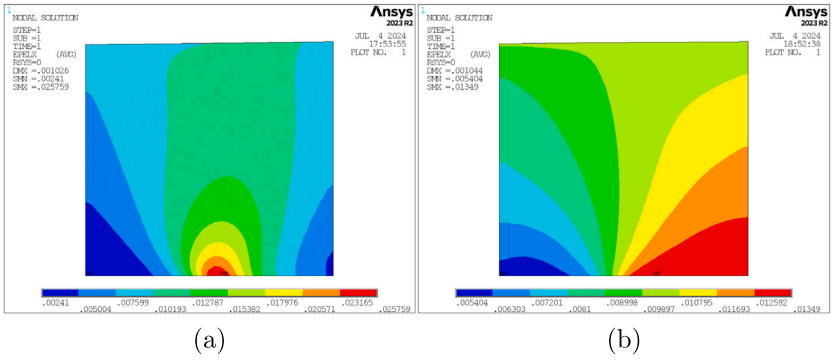

Fig. 11. Strain fields of the BVP II: (a) local approach; (b) global approach.

UserElem, which allowed for the practical application and validation of the proposed methodology.

The results of the numerical investigations have demonstrated that the outcomes of the local approach deviate from the expected results, particularly for significant curvatures of the print paths. Nevertheless, the introduction of a normalised local basis system has the capability to eliminate these undesirable phenomena. In terms of the reduction in simulation time compared to the conventional global approach, it can be observed that the local approach with a normalised basis has a certain potential, but does not have the same efficacy as the local approach with a covariant basis, which, however, leads to inaccurate results.

Further work may focus on extending this approach to three-dimensional problems for the application of multi-axial additive manufacturing, taking spatial print paths into account. In addition, the incorporation of more complex material models, such as those accounting for plasticity or viscoelasticity while taking the geometric nonlinearity into account, could broaden the applicability of the method. Furthermore, experimental validation using digital image correlation of the numerical results could further solidify the efficacy of the proposed approach in practical applications.

CRediT authorship contribution statement

Bruno Musil: Project administration, Conceptualization, Investigation, Methodology, Software, Validation, Writing – original draft. **Philipp Höfer:** Resources, Supervision, Writing – review & editing.

Declaration of competing interest

The authors declare that they have no known competing financial interests or personal relationships that could have appeared to influence the work reported in this paper.

Data availability

Data will be made available on request.

References

Betten, J., 1987. Tensorrechnung für Ingenieure. Springer.

Cinefra, M., 2022. Formulation of 3D finite elements using curvilinear coordinates. Mech. Adv. Mater. Struct. 29 (6), 879–888.
Fang, G., Zhang, T., Huang, Y., Zhang, Z., Masania, K., Wang, C.C., 2024. Exceptional mechanical performance by spatial printing with continuous fiber: Curved slicing, toolpath generation and physical verification. Addit. Manuf. 82, 104048.
Fernandez, F., Compel, W.S., Lewicki, J.P., Tortorelli, D.A., 2019. Optimal design of fiber reinforced composite structures and their direct ink write fabrication. Comput. Methods Appl. Mech. Engrg. 353, 277–307.
Fernandez, F., Lewicki, J.P., Tortorelli, D.A., 2021. Optimal toolpath design of additive manufactured composite cylindrical structures. Comput. Methods Appl. Mech. Engrg. 376, 113673.
Irgens, F., 2008. Continuum Mechanics. Springer Science & Business Media.
Irgens, F., Irgens, Baumann, 2019. Tensor Analysis. Springer.
Itskov, M., et al., 2007. Tensor Algebra and Tensor Analysis for Engineers. Springer.
Javili, A., McBride, A., Steinmann, P., Reddy, B., 2014. A unified computational framework for bulk and surface elasticity theory: a curvilinear-coordinate-based finite element methodology. Comput. Mech. 54, 745–762.
Kafle, A., Luis, E., Silwal, R., Pan, H.M., Shrestha, P.L., Bastola, A.K., 2021. 3D/4D printing of polymers: fused deposition modelling (FDM), selective laser sintering (SLS), and stereolithography (SLA). Polymers 13 (18), 3101.
Kiendl, J., Gao, C., 2020. Controlling toughness and strength of FDM 3D-printed PLA components through the raster layup. Composites B 180, 107562.
Klingbeil, E., 1966. Tensorrechnung für ingenieure. Verlag Anton Hain.
Klingenbeck, J., Lion, A., Johlitz, M., 2024. Investigation of the anisotropic mechanical behaviour of short carbon fibre-reinforced polyamide 6 fabricated via fused filament fabrication. In: Lectures Notes on Advanced Structured Materials, vol. 2, Springer, pp. 151–169.
Lachmeyer, R., Lippert, R., Fahlbusch, T., 2016. 3D-Druck beleuchtet: Additive Manufacturing auf dem Weg in die Anwendung. Springer Berlin Heidelberg, Berlin.
Murugan, V., Alaimo, G., Auricchio, F., Marconi, S., 2022a. An orientation-field based algorithm for free-form material extrusion. Addit. Manuf. 59, 103064.
Murugan, V., Alaimo, G., Marconi, S., Berke, P.Z., Massart, T.J., Auricchio, F., 2022b. Filament path optimization of Fused Filament Fabricated parts incorporating the effect of pre-fusion densities. Int. J. Solids Struct. 254, 111916.
Parandoush, P., Lin, D., 2017. A review on additive manufacturing of polymer-fiber composites. Compos. Struct. 182, 36–53.
Tekinalp, H.L., Kunc, V., Velez-Garcia, G.M., Duty, C.E., Love, L.J., Naskar, A.K., Blue, C.A., Ozcan, S., 2014. Highly oriented carbon fiber–polymer composites via additive manufacturing. Compos. Sci. Technol. 105, 144–150.
Valle, J.M., Albanesi, A., Fachinotti, V., 2019. An efficient general curvilinear coordinates finite element method for the linear dynamic study of thickness-independent shells. Latin Am. J. Solids Struct. 16 (05), e183.
VDI 3405, 2014. Additive Fertigungsverfahren, (3405).
Voelkl, H., Wartzack, S., 2021. Systematic development of load-path dependent FLM-FRP lightweight structures. Design Sci. 7, e10.
Witzgall, C., Völkl, H., Wartzack, S., 2022. Derivation and validation of linear elastic orthotropic material properties for short fibre reinforced FLM parts. J. Compos. Sci. 6 (4), 101.